Catalysis Science & Technology

PAPER

View Article Online
View Journal | View Issue

Cite this: *Catal. Sci. Technol.*, 2017, 7, 2245

CO_2 activation on Cu-based Zr-decorated nanoparticles†

Natalie Austin, Jingyun Ye and Giannis Mpourmpakis*

Density functional theory (DFT) calculations have been applied to investigate the electronic and CO_2 adsorption properties of 55-atom Cu-based nanoparticles (NPs) decorated with Zr atoms ($Cu_{55-x}Zr_x$, x = 0–12). Our results revealed that the Zr atoms preferably reside on the surface of the Cu NPs generating sites that chemisorb and activate CO_2 (linear to bent geometry and elongation of C═O bonds). Importantly, we demonstrate that while the CO_2 formation of the activated state on the Cu NPs is endothermic, it becomes barrierless and exothermic on the Zr-decorated NPs. The CO_2 activation and chemisorption was attributed to charge transferred from the NPs to the CO_2 molecule. We identified the local-site d-band center and, interestingly, the ionization potential of the NP as descriptors correlating with the CO_2 chemisorption. As a result, we demonstrate that one can tune the ionization potential of the NPs and, in turn the CO_2 chemisorption energy, by varying the Zr content of the NPs. Additionally, we investigated the activity of CuZr NPs as catalysts for CO_2 dissociation to CO and determined that $Cu_{54}Zr$ was a very efficient catalyst compared to Cu_{55}. Overall, this work highlights how surface decoration can change the electronic properties of the NPs and result in CO_2 activation, which are important steps for designing catalysts that capture and convert CO_2 to fuels and chemicals.

Received 16th December 2016,
Accepted 27th April 2017

DOI: 10.1039/c6cy02628a

rsc.li/catalysis

Introduction

Fossil fuel combustion has significantly led to elevated levels of carbon dioxide (CO_2) in the atmosphere, which in turn contributes to global warming through the greenhouse effect. Catalytic conversion of CO_2 to valuable products is of significant interest as a method to alleviate the effects of CO_2 on our environment.[1,2] The high thermodynamic stability of CO_2 limits its application in the chemical industry to a few processes including the synthesis of urea and carbonates.[3,4] However, the abundance and low-cost of CO_2 makes it an attractive carbon source to investigate its direct chemical transformation to other important products such as methanol (CH_3OH), formic acid, hydrocarbons, and carbon monoxide (CO).[1,5]

Atomic hydrogen serves as a highly reactive reducing species to convert CO_2 to relevant chemicals and fuels in hydrogenation reactions.[6–9] The direct dissociation of CO_2 to produce CO ($CO_2 \rightarrow CO^* + O^*$) can occur even in the absence of reducing species on transition metal (TM) surfaces.[10–12] Prior to its dissociation, CO_2 can exist in a bent state (activated state) on the catalyst surface.[12,13] This activated state is the result of charge transferred from the metal catalyst to the CO_2 molecule, which in turn results in the elongation of the C═O bonds and decrease in the O═C═O bond angle (linear to bent mode).[14,15] Spectroscopic studies have been instrumental in our understanding of CO_2 activation by identifying the formation of activated CO_2 on Ni(100) and K-doped Rh(111) surfaces prior to its dissociation.[12,16] In addition, theoretical investigations of CO_2 activation have been assessed on several metal and metal oxide catalysts.[10,11,13,17] In our recent DFT computational study we investigated the CO_2 adsorption on CuNi nanoparticles (NPs).[18] We found that NPs with surface Ni atoms strongly adsorbed CO_2 and that this chemisorption was accompanied by significant charge transfer to the CO_2 molecule leading to its activation.[18]

Focusing on CO_2 conversion to CH_3OH, CO_2 is contained in the syngas mixture (CO_2/CO/H_2) used for the industrial production of CH_3OH on Cu/ZnO/Al_2O_3 catalysts.[19] Experimental and theoretical studies have shown that CO_2 serves as the primary carbon source for the industrial synthesis of CH_3OH.[20,21] The active sites for CO_2 and CO hydrogenation on the industrial catalyst have been identified as a Cu stepped surface decorated with Zn atoms: a CuZn(211) surface.[22] CO and CO_2 hydrogenation intermediates were shown to exhibit increased adsorption strength and decreased barriers towards CH_3OH synthesis on CuZn(211) compared to the Cu(211) surface. The authors hypothesized that Zr, which

Department of Chemical Engineering, University of Pittsburgh, Pittsburgh, Pennsylvania 15261, USA. E-mail: gmpourmp@pitt.edu

† Electronic supplementary information (ESI) available. See DOI: 10.1039/c6cy02628a

has a similar oxophilicity to Zn can result in a similar adsorption behavior as observed with the decoration of Zn atoms on the surface of Cu(211).[22] In addition, experimental studies showed higher conversion and selectivity for CH_3OH from CO_2 hydrogenation on ZrO_2-doped Cu/ZnO catalysts compared to Cu/ZnO.[23] Thus, it appears that the incorporation of Zr into Cu-based catalysts results in generating more efficient catalysts for the chemical transformation of CO_2. To the best of our knowledge, theoretical investigations into the interactions of CO_2 on Cu-based Zr-decorated NPs (CuZr NPs) are absent from literature.

Since the activated state of CO_2 is a pertinent step for CO_2 conversion, it is important to identify catalytic systems designed to adsorb and activate CO_2 on their surfaces, which in turn contributes to designing more efficient CO_2 utilization technologies. In this work, we performed DFT calculations to examine the adsorption, activation, and reaction of CO_2 on 55-atom Cu NPs, with select surface Cu atoms being replaced by Zr atoms to generate Zr-decorated Cu NPs. Our work demonstrates that Zr-decorated Cu-based NPs can be very efficient catalysts to adsorb, activate, and convert CO_2. A detailed analysis on the electronic structure and adsorption properties of the catalyst as a function of surface decoration is provided which aids in designing novel CO_2-utilization nanocatalysts.

Computational details

All DFT calculations in this work were performed using the Quickstep program in the computational package, CP2K.[24] The calculations implemented the revised PBE (revPBE) functional and the double-ζ plus polarization (DZVP) basis set[25] in combination with the Goedecker, Teter, and Hutter (GTH) pseudopotentials[26] with a 400 Ry cutoff. Grimme's DFT-D3 method[27] was used to account for dispersion interactions. Icosahedral 55-atom Cu NPs decorated with Zr atoms, $Cu_{55-x}Zr_x$ (x = 0, 1, 2, 4, 6, 8, 10, 12), with and without adsorbed CO_2 were optimized in nonperiodic 30 × 30 × 30 $Å^3$ cubic cells until forces were less than 0.02 eV $Å^{-1}$. Optimized structures were verified as ground states with frequency calculations (absence of imaginary modes).

Eqn (1) was used to determine the core or shell preference of Zr in the $Cu_{54}Zr$ NP. This preference is defined as the segregation energy (SE) of a single heteroatom (Zr) from the core to the surface of the host NP (Cu), where negative values indicate Zr preference for the surface.

$$SE = E(Cu_{54}Zr_{(surface)}) - E(Cu_{54}Zr_{(core)}) \quad (1)$$

where $E(Cu_{54}Zr_{(surface)})$ is the total electronic energy of the fully optimized $Cu_{54}Zr$ NP in which one Cu atom is replaced by one Zr atom on the surface of Cu_{55}, and $E(Cu_{54}Zr_{(core)})$ is the corresponding electronic energy for the core atom replacement. As shown in Fig. 1 there are two distinct surface sites on the NP: coordination number (CN) 6, which is a corner site, and CN8, which is an edge site. The Zr atom in $Cu_{54}Zr_{(core)}$ is placed in the very central core atom of the NP which is a CN12 site.

Fig. 1 55-Atom Cu NP decorated with Zr at the three coordination sites (CN = 6, 8, 12) listed above the NP. The SE values for Zr residing on the CN8 and CN6 sites of the NP are listed below the NP. The Cu atoms are colored brown and the Zr atoms are in light blue.

Eqn (2) was used to calculate CO_2 adsorption (binding energy, BE) on the $Cu_{55-x}Zr_x$ NPs

$$BE = E_{NP\_CO_2} - E_{NP} - E_{CO_2} \quad (2)$$

where $E_{NP\_CO_2}$, E_{NP}, and E_{CO_2} are the total energies of NP with adsorbed CO_2, the isolated NP, and isolated CO_2 molecule, respectively. For all CO_2 adsorption cases, we considered parallel and perpendicular adsorption configurations (see Fig. S1† for illustrations of the adsorption configurations considered).

The climbing image nudged elastic band (CI-NEB) method[28] was used to identify potential barriers towards CO_2 activation and dissociation on the NPs. Transition states determined from the CI-NEB calculations were further verified by frequency calculations which identified a single imaginary mode along the reaction coordinate. The convergence criterion for the maximum force was set to 0.1 eV $Å^{-1}$. Bader[29] charge analysis was further employed to quantify the charge transferred from the NPs to the CO_2 molecule.

Results and discussion

Zr doping of Cu NPs

The thermodynamic preference for the surface enrichment of metal A over metal B in an AB alloy can be determined using the segregation energy (SE) of a single impurity (heteroatom) in a host system.[30,31] In order to determine the SE using eqn (1), we placed a Zr atom on three sites of the NP as shown in Fig. 1. Specifically, we replaced one Cu atom in the 55-atom Cu NP at the core, edge, and corner sites, with CNs 12, 8, and 6, respectively. We identified that Zr prefers to reside on the surface of the NP as indicated by the negative SE values for the CN6 and CN8 Zr-decorated structures (compared to the energy of the central core position) shown below the NPs in Fig. 1. Additionally, we determined that the CN6 site with a SE of −1.88 eV is the most preferred surface site for Zr to reside compared to CN8 which has a SE of −1.78 eV. The preference of Zr on the NP surface can be attributed to the larger atomic radius of Zr (1.60 Å)[32] compared to that of Cu (1.28 Å);[32] Zr resides on the surface to minimize strain effects on the NP. Our calculated SE preference for Zr on the Cu NP

surface agrees with the determined SE preference for Zr on the surface of Cu(111).[31]

CO_2 adsorption and activation on $Cu_{54}Zr$ and Cu_{55} NPs

CO_2 can interact with TM systems in a physisorbed state, where it retains the geometric properties of gas phase CO_2, and in a chemisorbed state, where it becomes bent (activated).[13,15,18] We performed geometry optimizations of CO_2 adsorbed on $Cu_{54}Zr$ starting with CO_2 at a physisorbed (~3.5 Å) and chemisorbed distance (~2.0 Å) from the NP surface. The most preferential adsorption site we found in both states was CO_2 interacting parallel to the edge of the $Cu_{54}Zr$ NP near the Zr atom (see Fig. 2(a)). The physisorption and chemisorption energies were calculated to be −0.13 and −1.29 eV, respectively. The physisorbed state retained the geometric properties of gas phase CO_2 (average C═O bond length: 1.18 Å and O═C═O bond angle: 179.3°) while the chemisorbed state significantly deviated from gas phase CO_2 (average C═O bond length: 1.29 Å and O═C═O bond angle: 126.5°). We also assessed the transition from the physisorbed to chemisorbed state to identify any potential barriers towards activation given the enhanced thermodynamic stability of CO_2. As shown in Fig. 2(a), the physisorbed and chemisorbed structures served as inputs to a CI-NEB calculation, with 6–8 replicas, which revealed that CO_2 activation on $Cu_{54}Zr$ NP is barrierless. In the absence of surface Zr, the adsorption of CO_2 in an activated state on the Cu_{55} NP was found to be +0.45 eV which is unfavorable compared to the weak physisorption of CO_2 on Cu_{55} (−0.059 eV). Weak adsorption of CO_2 on monometallic Cu surfaces has also been observed in previous experimental and theoretical studies.[11,13,33] Fig. 2(b) shows that the transition from physisorbed CO_2 to the activated state of CO_2 is barrierless but endothermic. These results indicate that surface Zr on Cu NPs can be an active site for CO_2 adsorption and activation, whereas, surface Cu sites are not.

CO_2 adsorption and activation on $Cu_{55-x}Zr_x$ (x = 2, 4, 6, 8, 10, 12)

Following the observed adsorption and activation of CO_2 on the $Cu_{54}Zr$ NP we investigated the CO_2 adsorption behavior on CuZr NPs with an increasing surface fraction of Zr atoms. We generated the CuZr NPs by systematically replacing Cu with Zr at all CN6 sites of the 55-atom icosahedral NP. We selected CN6 as the site for Zr doping based on our SE analysis which showed that Zr preferred to reside on the CN6 site of the $Cu_{54}Zr$ NP. As shown in Fig. 3(a) we gradually replaced 2–12 Cu atoms with Zr atoms in the NP in a symmetric manner to investigate the effects of increasing concentration of Zr in a Cu-based NP. CO_2 hydrogenation studies on Cu/ZrO_2 have shown that Cu sites are favorable for H_2 dissociation and ZrO_2 is necessary for the activation of CO_2.[34,35] Thus, from a catalyst design perspective, our model for Zr doping of the Cu NP with the Zr atoms being at maximum separation, maximizes the available Zr sites for CO_2 activation, while keeping neighboring Cu sites for H_2 dissociation. We do note however that there may be more stable forms of $Cu_{55-x}Zr_x$ decoration other than decoration on the CN6 sites (see ESI† Fig. S2 for the case of $Cu_{53}Zr_2$ and corresponding CO_2 binding). Fig. 3(b) illustrates CO_2 BE as a function of surface fraction of Zr in the 55-atom NP. The observed CO_2 BE does not change significantly with the addition of 2–6 Zr atoms on the NP surface (BE range: −1.39 eV to −1.42 eV). In contrast, we observe a significant enhancement in the CO_2 BE with increasing Zr content when 8–12 Zr atoms are added on the NP surface (BE range: −1.52 eV to −1.80 eV). As shown in Fig. 4(a), for each $Cu_{55-x}Zr_x$ NP we observed activation of CO_2 by elongation of the C═O bonds and decrease in the O═C═O angle. Fig. 4(a) also demonstrates that the largest deviation of the geometrical features of CO_2 compared to the gas phase occurs on the NPs exhibiting the strongest BEs. The activation of CO_2 has been attributed to the charge transferred from the d-orbitals of the TM system to the anti-bonding orbitals of the CO_2 molecule.[14,15] Therefore in Fig. 4(b) we plotted the CO_2 BE as a

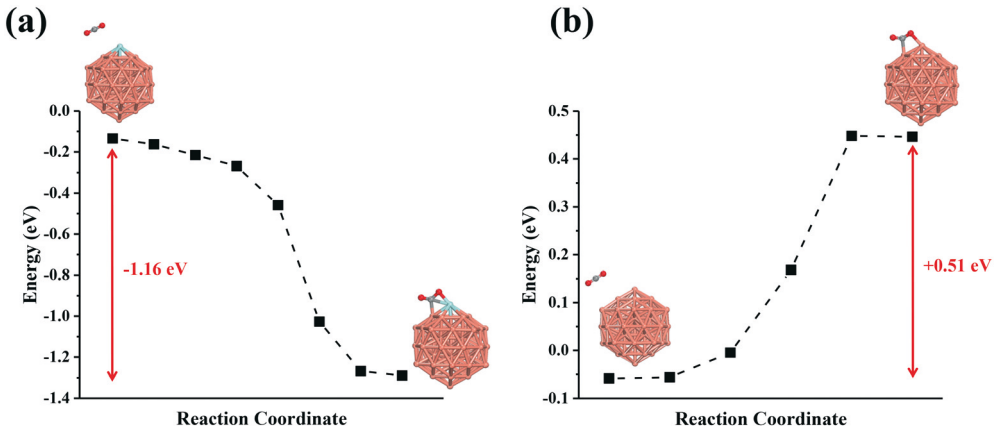

Fig. 2 CI-NEB calculations for the physisorbed to activated state of CO_2 on the (a) $Cu_{54}Zr$ and (b) Cu_{55} NP. The values in red in (a) and (b) is the change in energy (ΔE) from the physisorbed to activated state of CO_2 ($\Delta E = E_{activated} - E_{physisorbed}$). The negative (red) value in (a) represents an exothermic step, whereas, the positive value in (b) represents an endothermic step. The color code on the structure is as in Fig. 1, with the addition of CO_2 (C colored gray and O red).

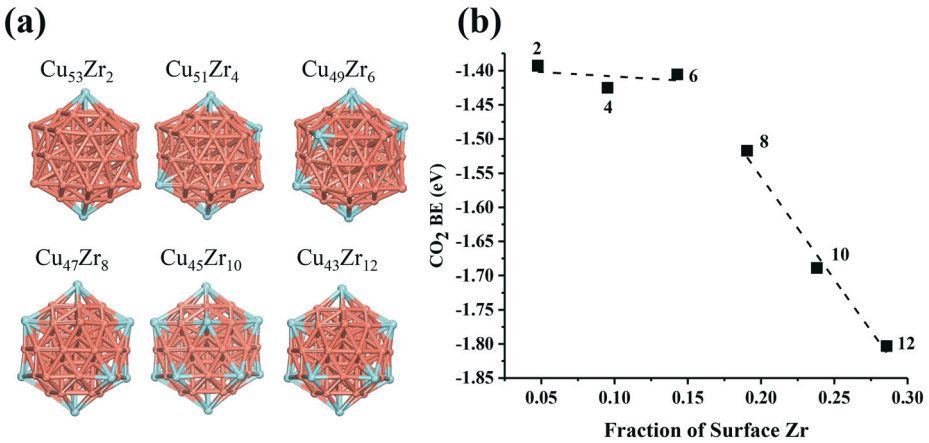

Fig. 3 (a) $Cu_{55-x}Zr_x$ (x = 2, 4, 6, 8, 10, 12) decoration on the 55-atom NPs. The color code is as in Fig. 1. (b) CO_2 adsorption as a function of surface fraction of Zr on the $Cu_{55-x}Zr_x$ NPs. The dashed lines serve as a guide to the eye.

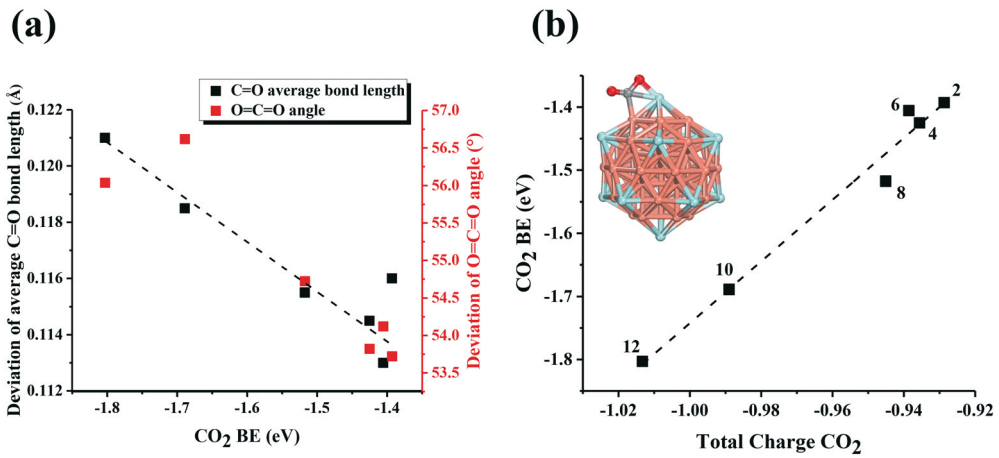

Fig. 4 (a) Deviation of adsorbed CO_2 geometric properties from gas phase CO_2. (b) CO_2 BE as a function of total charge on CO_2 for each $Cu_{55-x}Zr_x$ (x = 2, 4, 6, 8, 10, 12) NP. The inset figure shows chemisorbed CO_2 on $Cu_{43}Zr_{12}$. The color code for the inset is as in Fig. 2. The dashed lines in (a) and (b) serve as a guide to the eye.

function of the total charge located on the activated CO_2 bound to the Zr-decorated Cu NPs. We found that for each NP case more than 0.9 $|e|$ charge was transferred to the CO_2 molecule from the NP. It should be noted that to verify that the activated (chemisorbed) state of CO_2 remains barrierless on the NPs with the high Zr content, we performed CI-NEB calculations on the $Cu_{43}Zr_{12}$ NP, which has the highest composition of Zr in our study and found that indeed, the CO_2 chemisorption remains barrierless and exothermic.

Electronic properties of the CuZr NPs

An understanding of the underlying catalyst properties responsible for CO_2 activation is important for developing catalysts with enhanced CO_2 conversion activity. Therefore, we assessed the d-band center (d_C) and ionization potential (IP) as NP descriptors for our observed adsorption trends. Hammer and Nørskov have shown that the d_C of a metal catalyst can be correlated with the adsorbate BE.[36,37] In addition, we have previously shown that the IP of a catalyst (or equivalently work function) is a good descriptor for adsorption[38] especially for systems involving charge transfer (case of CO_2 interaction as shown in Fig. 4(b)). In Fig. 5(a) we identified a correlation between the CO_2 BE and the localized d_C of the Zr atom interacting with CO_2 for each $Cu_{55-x}Zr_x$ NP (see inset in Fig. 4(b)). In the ESI† (Fig. S3), we illustrate the PDOS used to determine the d_C for each NP. It is important to note that for $Cu_{55-x}Zr_x$ NPs with 2–6 Zr atoms on the surface we observe a negligible change in the d_C of the site, which in turn results to a practically unaffected CO_2 BE as shown in Fig. 3(a). Conversely, for $Cu_{55-x}Zr_x$ NPs with 8–12 Zr atoms the d_C varied more significantly and in turn, there were significant variations in the CO_2 BE. We also observe from Fig. 5(a) that as we increase the Zr composition, the d_C shifts closer to the Fermi level (*i.e.* a shift closer to zero in Fig. 5(a)) which is responsible for the increasing adsorption strength of CO_2.

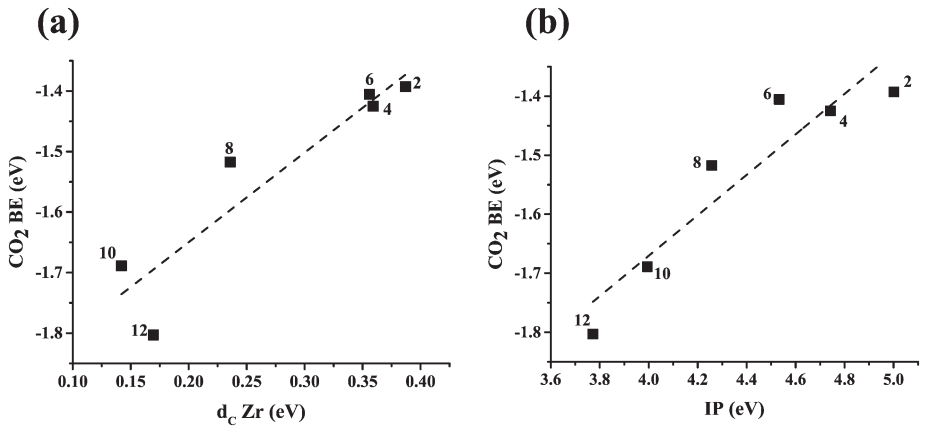

Fig. 5 CO_2 BE as a function of (a) d_C of Zr atoms and (b) the IP for each of the $Cu_{55-x}Zr_x$ (x = 2, 4, 6, 8, 10, 12) NPs.

Overall, the local d_C appears to be a good descriptor for the observed CO_2 adsorption behavior. In Fig. 5(b) we present the relationship between the CO_2 BE and the IP of the NP. As the IP decreases we observe a stronger CO_2 BE. Given that the IP represents the ability of the NP to donate electrons, we believe that the IP is the catalyst property responsible for the degree of charge transfer to the CO_2 molecule resulting in the activation of the molecule. In addition, Fig. 5(b) demonstrates a way to tune CO_2 chemisorption: increasing the surface Zr composition (experimental parameter) decreases the IP of the NP, and in turn, the CO_2 adsorption becomes stronger. As shown in Fig. S3 of the ESI† file, increasing the Zr composition, shifts the HOMO (highest occupied molecular orbital) towards the LUMO of CO_2 (lowest unoccupied molecular orbital) and closer to the Fermi level of the NP. This in turn, results to decreasing the catalyst IP and increasing the interaction energy of CO_2.

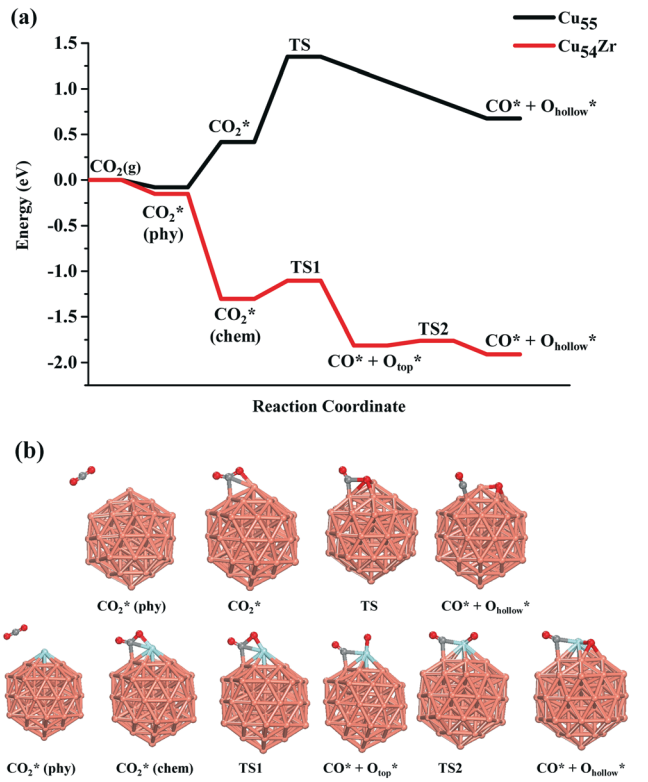

Fig. 6 (a) CO_2 dissociation reaction path on Cu_{55} (black line) and $Cu_{54}Zr$ (red line). For Cu_{55}, TS represents breaking of a C–O bond, with a C–O bond length of 1.87 Å. For $Cu_{54}Zr$, TS1 represents the breaking of a C–O bond, with a C–O bond length of 1.73 Å and TS2 represents the diffusion of O from a top site to hollow site configuration. (b) Optimized structures for the CO_2 dissociation to CO and O on the Cu_{55} (top row) and $Cu_{54}Zr$ (bottom row) NPs.

CO_2 dissociation to CO on $Cu_{55}Zr$ *vs.* Cu_{55}

The facile chemisorption of CO_2 on the $Cu_{55-x}Zr_x$ NPs indicates that the NPs could serve as favorable CO_2 reduction catalysts compared to monometallic Cu NPs alone. As a preliminary analysis, for our ongoing CO_2 reaction studies, we compared the CO_2 dissociation barriers on $Cu_{54}Zr$ and Cu_{55} and found that $Cu_{54}Zr$ dissociated CO_2 at a significantly lower barrier than Cu_{55}. Specifically, Fig. 6(a) illustrates the dissociation of CO_2 into adsorbed CO and O on both the Cu_{55} and $Cu_{54}Zr$ NPs relative to the isolated CO_2 molecule and the NP. We found that the transition state (TS) energy value and bond length for C–O bond breaking on Cu_{55} and $Cu_{54}Zr$ are 0.93 eV and 1.87 Å, and 0.20 eV and 1.73 Å, respectively. The second TS in the $Cu_{54}Zr$ pathway, which has a small barrier of 0.05 eV represents the diffusion of O from a top site to a slightly more stable hollow site configuration. The $Cu_{54}Zr$ system exhibits the second TS because the direct transition of O into the hollow site from CO_2 dissociation through a single TS (as was for Cu_{55}) was not favorable. The corresponding structures for each state of the energy diagram are shown in Fig. 6(b).

Conclusions

In summary, we investigated the electronic and CO_2 adsorption properties of $Cu_{55-x}Zr_x$ (x = 0, 1, 2, 4, 6, 8, 10, 12) NPs. These Cu-based NPs, which consist of 55-atoms, have a decorated distribution of Zr atoms on the surface. Segregation energy analysis identified that Zr prefers to reside on the surface of the NPs, especially at the lower coordinated sites.

Adsorption calculations revealed that the Zr site at the NP surface is the most favorable site for CO_2 adsorption. The CO_2 binding energy varies slightly when the decorated Zr increases from 2 to 6 atoms on the Cu NP surface. However, a significant increase in the CO_2 binding energy was observed when we decorated 8–12 Zr atoms on the Cu NP surface. Furthermore, the elongation of C═O bond lengths and the bending of O═C═O bond angles were observed for all CO_2 adsorption cases on the $Cu_{55-x}Zr_x$ NPs, which indicates that CO_2 is activated when it adsorbs on $Cu_{55-x}Zr_x$ NPs (compared to the linear gaseous CO_2). We found the chemisorption of CO_2 on the Zr-decorated Cu NPs to be barrierless and exothermic, while it is endothermic on monometallic Cu_{55} NP. This chemisorption behavior was attributed to a strong charge transfer from the CuZr NPs to CO_2, resulting in the activation of CO_2. We further identified two descriptors for CO_2 adsorption: the d-band center (d_C) localized on the Zr atom interacting with CO_2 and the ionization potential (IP) of the whole NP. Both descriptors correlate with the CO_2 adsorption energies. The latter descriptor is significant since it can be experimentally measured and, as we demonstrate in this work, it can be tuned with the Zr content (composition variation) on the NP surface. To assess the effectiveness of CuZr NPs as catalysts for CO_2 conversion, we investigated the CO_2 dissociation to CO and O on $Cu_{54}Zr$ and Cu_{55}. We found that the barriers towards CO_2 dissociation on the $Cu_{54}Zr$ NP were much lower than that on the Cu_{55} NP. Our work demonstrates that Zr-decorated Cu-based NPs enhance the adsorption and activation of CO_2, which in turn, results in lower barriers towards the dissociation of CO_2. Overall, this work provides guidelines for the design of potentially promising catalysts for CO_2 conversion to valuable fuels and chemicals.

Acknowledgements

This material is based upon work supported by the National Science Foundation under Grant No. CMMI 1634880. N. A. would like to acknowledge support from the National Science Foundation Graduate Research Fellowship Program under Grant No. 1247842. The authors would also like to acknowledge computational support from XSEDE and the Center for Simulation and Modeling (SAM) at the University of Pittsburgh.

References

1 W. Wang, S. P. Wang, X. B. Ma and J. L. Gong, *Chem. Soc. Rev.*, 2011, **40**, 3703–3727.
2 Y. W. Li, S. H. Chan and Q. Sun, *Nanoscale*, 2015, 7, 8663–8683.
3 M. Aresta and A. Dibenedetto, *Dalton Trans.*, 2007, 2975–2992, DOI: 10.1039/b700658f.
4 R. Zevenhoven, S. Eloneva and S. Teir, *Catal. Today*, 2006, **115**, 73–79.
5 G. Centi, E. A. Quadrelli and S. Perathoner, *Energy Environ. Sci.*, 2013, **6**, 1711–1731.
6 J. Y. Ye, C. J. Liu, D. H. Mei and Q. F. Ge, *J. Catal.*, 2014, **317**, 44–53.
7 C. Tisseraud, C. Comminges, S. Pronier, Y. Pouilloux and A. Le Valant, *J. Catal.*, 2016, **343**, 106–114.
8 M. M. J. Li, Z. Y. Zeng, F. L. Liao, X. L. Hong and S. C. E. Tsang, *J. Catal.*, 2016, **343**, 157–167.
9 S. Kuld, M. Thorhauge, H. Falsig, C. F. Elkjaer, S. Helveg, I. Chorkendorff and J. Sehested, *Science*, 2016, **352**, 969–974.
10 Q. L. Tang, Q. J. Hong and Z. P. Liu, *J. Catal.*, 2009, **263**, 114–122.
11 C. Liu, T. R. Cundari and A. K. Wilson, *J. Phys. Chem. C*, 2012, **116**, 5681–5688.
12 F. Solymosi, *J. Mol. Catal.*, 1991, **65**, 337–358.
13 J. Ko, B. K. Kim and J. W. Han, *J. Phys. Chem. C*, 2016, **120**, 3438–3447.
14 S. G. Wang, X. Y. Liao, D. B. Cao, C. F. Huo, Y. W. Li, J. G. Wang and H. J. Jiao, *J. Phys. Chem. C*, 2007, **111**, 16934–16940.
15 H. J. Freund and M. W. Roberts, *Surf. Sci. Rep.*, 1996, **25**, 225–273.
16 F. Solymosi and G. Klivenyi, *Surf. Sci.*, 1994, **315**, 255–268.
17 K. R. Hahn, M. Iannuzzi, A. P. Seitsonen and J. Hutter, *J. Phys. Chem. C*, 2013, **117**, 1701–1711.
18 N. Austin, B. Butina and G. Mpourmpakis, *Prog. Nat. Sci.: Mater. Int.*, 2016, **26**, 487–492.
19 M. Behrens, *J. Catal.*, 2009, **267**, 24–29.
20 F. Studt, M. Behrens, E. L. Kunkes, N. Thomas, S. Zander, A. Tarasov, J. Schumann, E. Frei, J. B. Varley, F. Abild-Pedersen, J. K. Nørskov and R. Schlogl, *ChemCatChem*, 2015, **7**, 1105–1111.
21 L. C. Grabow and M. Mavrikakis, *ACS Catal.*, 2011, **1**, 365–384.
22 M. Behrens, F. Studt, I. Kasatkin, S. Kuehl, M. Haevecker, F. Abild-Pedersen, S. Zander, F. Girgsdies, P. Kurr, B.-L. Kniep, M. Tovar, R. W. Fischer, J. K. Nørskov and R. Schloegl, *Science*, 2012, **336**, 893–897.
23 C. Yang, Z. Y. Ma, N. Zhao, W. Wei, T. D. Hu and Y. H. Sun, *Catal. Today*, 2006, **115**, 222–227.
24 J. VandeVondele, M. Krack, F. Mohamed, M. Parrinello, T. Chassaing and J. Hutter, *Comput. Phys. Commun.*, 2005, **167**, 103–128.
25 J. VandeVondele and J. Hutter, *J. Chem. Phys.*, 2007, **127**, 114105.
26 S. Goedecker, M. Teter and J. Hutter, *Phys. Rev. B: Condens. Matter Mater. Phys.*, 1996, **54**, 1703–1710.
27 S. Grimme, J. Antony, S. Ehrlich and H. Krieg, *J. Chem. Phys.*, 2010, **132**, 154104.
28 G. Henkelman, B. P. Uberuaga and H. Jonsson, *J. Chem. Phys.*, 2000, **113**, 9901–9904.
29 G. Henkelman, A. Arnaldsson and H. Jonsson, *Comput. Mater. Sci.*, 2006, **36**, 354–360.
30 L.-L. Wang and D. D. Johnson, *J. Am. Chem. Soc.*, 2009, **131**, 14023–14029.
31 A. V. Ruban, H. L. Skriver and J. K. Nørskov, *Phys. Rev. B: Condens. Matter Mater. Phys.*, 1999, **59**, 15990–16000.
32 C. Kittel, *Introduction to Solid State Physics*, Wiley, New York, 7th edn, 1996.

33 E. Vesselli, E. Monachino, M. Rizzi, S. Furlan, X. M. Duan, C. Dri, A. Peronio, C. Africh, P. Lacovig, A. Baldereschi, G. Comelli and M. Peressi, *ACS Catal.*, 2013, **3**, 1555–1559.
34 F. Arena, G. Italiano, K. Barbera, S. Bordiga, G. Bonura, L. Spadaro and F. Frusteri, *Appl. Catal., A*, 2008, **350**, 16–23.
35 Q. J. Hong and Z. P. Liu, *Surf. Sci.*, 2010, **604**, 1869–1876.
36 B. Hammer and J. K. Nørskov, in *Advances in Catalysis, Vol 45: Impact of Surface Science on Catalysis*, ed. B. C. Gates and H. Knozinger, 2000, vol. 45, pp. 71–129.
37 B. Hammer and J. K. Nørskov, *Surf. Sci.*, 1995, **343**, 211–220.
38 A. N. Andriotis, G. Mpourmpakis, S. Broderick, K. Rajan, S. Datta, M. Sunkara and M. Menon, *J. Chem. Phys.*, 2014, **140**, 8.